Quaternary Research (2021), **102**, 175–187
doi:10.1017/qua.2020.126

Research Article

Holocene ice wedge formation in the Eureka Sound Lowlands, high Arctic Canada

Kethra Campbell-Heaton[a], Denis Lacelle[a]*, David Fisher[b] and Wayne Pollard[c]

[a]Department of Geography, Environment and Geomatics, University of Ottawa, Ottawa, Ontario, K1N 6N5, Canada; [b]Department of Earth and Environmental Sciences, University of Ottawa, Ottawa, Ontario, K1N 6N5, Canada and [c]Department of Geography, McGill University, Montreal, Quebec, H3A 0B9, Canada

Abstract

Ice wedges are ubiquitous periglacial features in permafrost terrain. This study investigates the timing of ice wedge formation in the Fosheim Peninsula (Ellesmere and Axel Heiberg Islands). In this region, ice wedge polygons occupy ~50% of the landscape, the majority occurring below the marine limit in the Eureka Sound Lowlands. Numerical simulations suggest that ice wedges may crack to depths of 2.7–3.6 m following a rapid cooling of the ground over mean winter surface temperatures of −18°C to −38°C, corresponding to the depth of ice wedges in the region. The dissolved organic carbon (DOC)/Cl molar ratios suggest that the DOC in the ice wedges is sourced from snowmelt and not from leaching of the active layer. Based on 32 $^{14}C_{DOC}$ measurements from 15 ice wedges, the wedges were likely developing between 9000–2500 cal yr BP. This interval also corresponds to the period of peat accumulation in the region, a proxy of increased moisture. Considering that winter air temperatures remained favorable for ice wedge growth throughout the Holocene, the timing of ice wedge formation reflects changes in snowfall. Overall, this study provides the first reconstruction of ice wedge formation from a high Arctic polar desert environment.

Keywords: Ground ice, permafrost, radiocarbon dating, Arctic

(Received 8 September 2020; accepted 15 December 2020)

INTRODUCTION

Ice wedges and associated tundra polygons are a ubiquitous feature of permafrost terrain (French, 2013). The density, size, and overall activity of ice wedges vary as a function of climate, vegetation, and polygon morphometry (Mackay, 1974, 1992, 1993; Fortier and Allard, 2005; Abolt et al., 2018). Early research on ice wedges focused on their growth and the mechanics of cracking in relation to winter conditions (Lachenbruch, 1962). Ice wedges tend to develop when winter ground surface temperatures are < −10°C and when the tensile strength of the ice is exceeded during thermal contraction following rapid cooling (Mackay, 1993; Fortier and Allard, 2005). Most ice wedges crack between mid-January to late March near the center, with a crack width in the 2–4 cm range and a crack depth that approximates the depth of the wedge (Mackay, 1974). The frequency of ice wedge cracking is variable, ranging from annual to decadal, and depends primarily on winter air and ground temperatures, the latter being dependent on snow depth, vegetation, and polygon morphology (Liljedahl et al., 2016). Mackay (1974) observed that narrow (<1 m) and wide (>2 m) ice wedges have lower cracking frequencies due to competing cracking and a reduction of thermal stress caused by the insolating effect of a greater snow cover in a wider trough, respectively. Once a crack is formed, it can be infilled by a variety of moisture sources, the most common being snow meltwater, but vapor condensation (hoarfrost) and snow have been observed as well (Lauriol et al., 1995; French and Guglielmin, 2000; St-Jean et al., 2011). The annual growth increment of an ice wedge can vary from <1 mm to a few millimeters, much smaller than the width of a winter crack due to thermal expansion (Mackay, 1974; Lewkowicz, 1994).

With recent advances in radiocarbon dating of dissolved organic carbon ($^{14}C_{DOC}$), Lachniet et al. (2012) demonstrated that measurements of $^{14}C_{DOC}$ greatly reduced the potential contamination of older particulate organic carbon in the ice wedge. To date, $^{14}C_{DOC}$ chronologies of ice wedge formation are all from western Arctic Canada and they provide insights into periods when winter temperatures and snow depth were favorable to both ice wedge cracking and growth (see Grinter et al., 2019; Holland et al., 2020). For example, the $^{14}C_{DOC}$ time series of ice wedges on the Blackstone Plateau in central Yukon showed that the wedges were developing when winter temperatures were cold and with sufficient snow to allow their growth and were not active during the warm early Holocene interval (Grinter et al., 2019). Despite the chronology of ice wedge formation in western Arctic Canada, the timing of the formation of ice wedges over the late Quaternary in other permafrost regions is largely unknown. In high Arctic Canada, ice wedge polygons occupy ~50% of the Fosheim Peninsula (Nunavut, Canada), with most situated below the Holocene marine limit in the Eureka Sound Lowlands (ESL) (Couture and Pollard, 1998; Bernard-Grand'Maison and Pollard, 2018), Despite studies documenting

*Corresponding author: Department of Geography, Environment and Geomatics, University of Ottawa, Ottawa, Ontario, Canada. E-mail address: dlacelle@uottawa.ca (*D. Lacelle*).

Cite this article: Campbell-Heaton K, Lacelle D, Fisher D, Pollard W (2021). Holocene ice wedge formation in the Eureka Sound Lowlands, high Arctic Canada. *Quaternary Research* **102**, 175–187. https://doi.org/10.1017/qua.2020.126

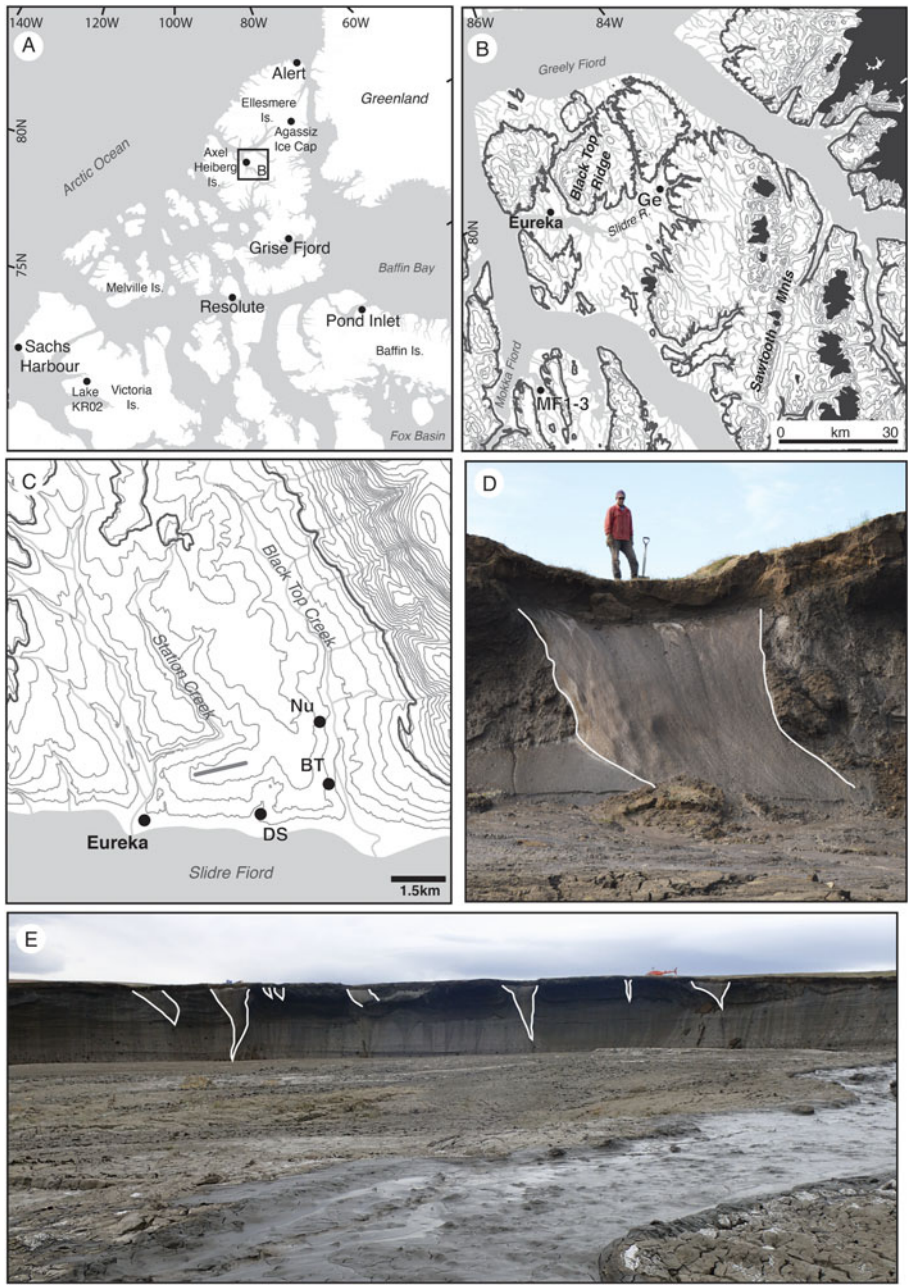

Fig. 1. (color online) Location of ice wedges sampled in the Eureka Sound Lowlands, high Arctic Canada. (A–C) Maps showing sampling sites around Eureka (Gemini, Nunavut, Blacktop, and Dump slumps) and Mokka Fjord. (D and E) Field photographs of ice wedges sampled in headwall of thaw slumps at Blacktop slump (D) and Mokka Fjord (E).

the recent degradation of ice wedge polygons in the region (Becker et al., 2016; Ward Jones et al., 2020), the timing of the formation of ice wedges in this polar desert region is unknown, especially in relation to the marine regression, permafrost aggradation, and Holocene climate.

This study investigates the timing Holocene ice wedge formation in the ESL based on 32 $^{14}C_{DOC}$ measurements from 15 wedges situated along an elevation gradient from near sea level to the Holocene marine limit. Considering that air temperatures in the high Arctic were always favorable to the growth of ice wedges (mean annual air temperature < −12°C; mean winter air temperature < −30°C; Lecavalier et al., 2017; Buizert et al., 2018), we hypothesize that the formation ice wedge reflects changes in snow, which would affect the winter ground surface temperature. The objective is achieved by: (1) modeling cracking of ice wedges based on simulations of stress buildup in ice wedges following rapid cooling for a range of ground surface temperatures; (2) determining the source of moisture and DOC in the ice wedges by comparing δD-$\delta^{18}O$, DOC/Cl, and $\delta^{13}C_{DOC}$ to those in residual snow and leached active layer soils; (3) assessing the cracking frequency and period of growth of the ice wedges based on the width and $^{14}C_{DOC}$ measurements of the wedges and the Mackay (1974) cracking probability model; and (4) comparing the ^{14}C age distribution of ice wedges with regional Holocene air temperature and precipitation reconstructions and periods of peat accumulation.

Study area

The ESL is an intermontane basin on the Fosheim Peninsula situated in the west-central section of Ellesmere Island and the southeastern section of Axel Heiberg Island (Fig. 1). The region

https://doi.org/10.1017/qua.2020.126 Published online by Cambridge University Press

consists of flat to gently rolling terrain situated at elevations <200 m above sea level (m asl) and is underlain by the Sverdrup Basin, a folded and faulted Carboniferous to Paleogene sedimentary bedrock composed of sandstone, siltstone, and shale strata (Bell, 1996; Hodgson and Nixon, 1998).

The late Quaternary glacial history of the Queen Elizabeth Islands has long been debated with contrasting views. The most recent glacial history reconstruction suggests that the Innuitian Ice Sheet covered most of the Queen Elizabeth Islands and reached its maximum extent at about 15,800 ^{14}C yr BP, with the ice being 1.6 km thick in the ESL (Dyke et al., 2002; England et al., 2006). Deglaciation started between 10,300–8800 ^{14}C yr BP (England et al., 2006), and remnants of the ice sheet are still found at the nearby Agassiz Ice Cap. Marine transgression followed until 8800–7800 ^{14}C yr BP, with the Holocene marine limit found between 139 and 150 m asl (Bell, 1996). The surficial sediments on the Fosheim Peninsula reflect the regional glacial history, with weathered bedrock, till, and glaciofluvial sediments found above the marine limit and early Holocene–age marine deposits found along the lowlands below the marine limit (Hodgson and Nixon, 1998; Bell and Hodgson, 2000). Solifluction, rill washing, and slope failures reworked these deposits into colluvium deposits along hillslopes (Bell and Hodgson, 2000).

The ESL is characterized by a polar desert climate, with cold winter and cooler summer air temperatures than inland locations. The 1980–2016 mean annual air temperature recorded at the Eureka weather station, situated within 50 km of all study sites, was −18.5 ± 1.4°C; mean winter air temperature was −38.5 ± 1.7°C; mean summer air temperature was 4.3 ± 1.3°C (Environment Canada, 2019). Total precipitation reaches 77.6 ± 25.8 mm/yr, with 80% falling as snow. Late winter snow depth ranges from 5 to 35 cm, although it is likely thicker in well-developed polygonal troughs. The low precipitation compared with other sites in the high Arctic is attributed to the surrounding topography, which blocks cold ocean air masses and creates a rain shadow (Edlund and Alt, 1989). Vegetation is composed of patchy graminoid and prostrate dwarf-shrub (Edlund et al., 2000). Holocene air temperatures were reconstructed from δ^{18}O measurements from the Agassiz Ice Cap. The 25-yr mean annual air temperature record shows a rapid early Holocene warming with temperatures being 6°C warmer than today at 10 ka followed by a gradual cooling to AD 1700 (Lecavalier et al., 2017). Presently, air temperatures are rapidly warming and are now at their warmest in the past 6800–7800 yr (Lecavalier et al., 2017; Copland et al., 2020). The 20-yr winter air temperature reconstruction follows a similar pattern to the mean annual one, with winter temperatures reaching about −30°C in the early Holocene, although this reconstruction does not include the correction for change in surface elevation (Buizert et al., 2018).

The climate and vegetation conditions ensure that permafrost is cold, continuous, and ~500 m thick (Pollard, 2000). The active layer thickness averages 60 cm (Hodgson and Nixon, 1998; Couture and Pollard, 2007) and the mean annual ground temperature (measured at 15.4 m, the depth of zero annual amplitude) is −16.5°C (Pollard et al., 2015). Ice wedge polygons are the main periglacial landform and are mostly found within the Holocene marine limit (Couture and Pollard, 1998; Bernard-Grand'Maison and Pollard, 2018). The ice wedges are mostly epigenetic (Pollard, 1991), but syngenetic wedges can be found in places of recent colluviation, with ice wedge growth estimated at 1.9–4.8 mm/yr from tritium analyses (Lewkowicz, 1994). Based on a survey of 150 ice wedges, their average width and depth are 1.46 ± 0.56 m and 3.23 ± 0.8 m, respectively (Couture and Pollard, 1998).

METHODS

Modeling cracking of ice wedges

Numerical simulations were conducted using the REGO model to test for the effects of past warmer ground surface temperatures (either warmer winters or thicker snow cover) on ice wedge cracking in the ESL. REGO is a soil environmental model that uses as input a series of parameters related to the soil temperature, porosity, and permeability and soil water chemistry (Fisher, 2005; Fisher and Lacelle, 2014; Fisher et al., 2020). The model solves for coupled frozen soil stresses using the thermophysical characteristics of the soils (i.e., dry porosity, density, tortuosity, thermal diffusivity), the mean ground surface temperature and its amplitude, the period of the temperature cycle, and the geothermal gradient. The theory behind temperature waves of a given period to generate various stress fields in icy soils has been explained in detail in other studies (e.g., Lachenbruch, 1962).

The cracking depth in ice wedges developed in icy soils was modeled for initial ground surface temperatures of −38°C, −28°C, −18°C, and −8°C. REGO uses as input a cyclic temperature; therefore, to simulate a rapid decrease in temperature, the ground surface was cooled by 8°C or 17°C with a periodicity of 1/16 of a year (or 23 days, equivalent to cooler temperature below the mean lasting ca. 6 days). This periodicity represents the typical time scale for weather systems to move through a given region (ca. 10 days; e.g., Hoskins et al., 1983). Simulating a faster or slower thermal change does not greatly affect the stress fields. The simulations were performed with a soil thermal diffusivity of 62 m^2/yr and treat the icy soil and ice as a Maxwellian viscoelastic solid subject to elastic and thermal strains. The [1] decaying temperature wave that propagates into the icy permafrost and ice wedge, [2] the associated thermal expansion, and [3] the resulting elastic and creep strains were used to determine the nonhydrostatic stress field. The ice wedge (pure ice) will typically crack when tension exceeds ~0.4–0.6 MPa; icy soils will typically crack when tension exceeds 1.5–2 MPa (Williams and Smith, 1989).

Field sampling of ice wedges

Epigenetic ice wedges were sampled in July 2019 from the headwall of five thaw slumps situated between the Holocene marine limit and the coastline: Gemini (120 m), Nunavut (73–100 m), Black Top (60–66 m), Mokka Fjord (55–58 m), and Dump (34–36 m) (Fig. 1). At the Nunavut, Blacktop, and Mokka Fjord slumps, the ice wedges developed in ice-rich, silty-clay marine sediments, whereas at Gemini and Dump slumps, the ice wedges developed in tabular bodies of massive ice.

Depending on accessibility, two to five ice wedges were sampled from each site. The ice wedges were sampled by first removing the overlying active layer soil and exposing the full width of the wedge. Each ice wedge was then cored from its center and near the edges using a mini-CRREL coring kit. The ice wedges were cored from their surfaces to 30 cm depths, and all samples were wrapped in aluminum foil and kept frozen in a chest freezer in Eureka. The active layer soil above each ice wedge was sampled at 5 cm intervals in Ziploc bags. Residual

https://doi.org/10.1017/qua.2020.126 Published online by Cambridge University Press

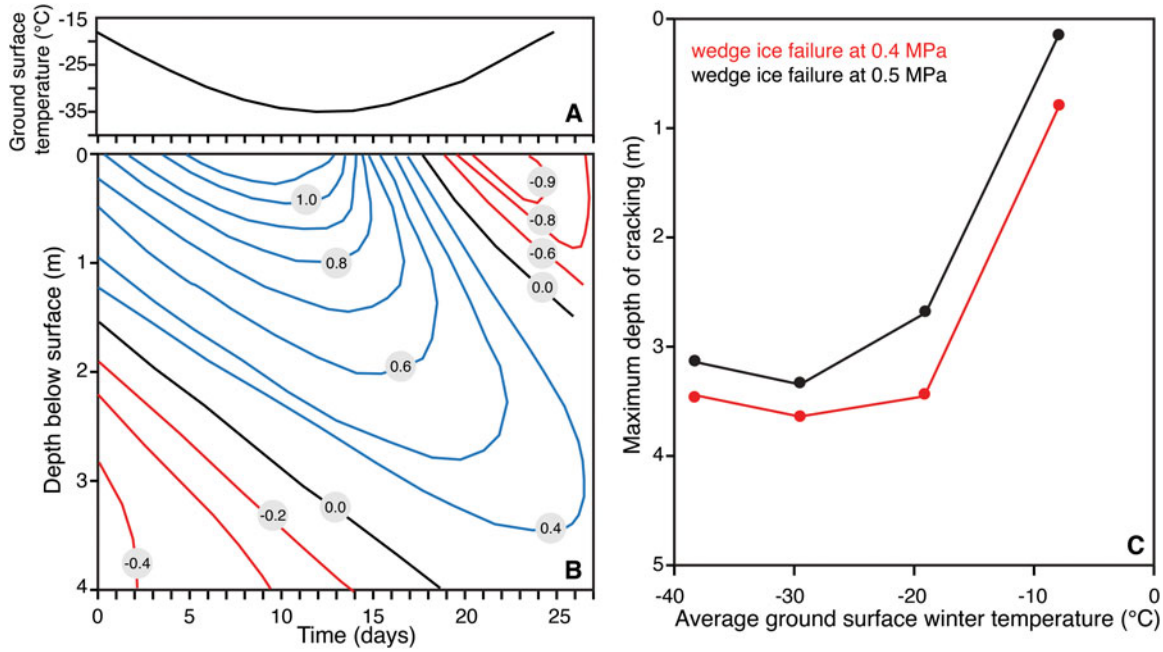

Fig. 2. (color online) Stress field and cracking depth in icy permafrost as a function of mean winter ground surface temperatures. (A) An example of simulated winter ground surface temperature with average of −18°C subjected to a decrease of 17°C around a period of 1/16 of a year. (B) The stress field that results from the rapid cooling of winter ground surface temperature averaging −18°C. Tensions are indicated as positive numbers, and pressures are negative numbers. The stresses are generated in the icy permafrost (thermal diffusivity of 62 m^2/yr), and these are assumed to be the same in the ice wedge. The icy permafrost itself will not crack until the tension stresses reach about 1.5 MPa, but the ice wedge would crack when tension reaches 0.4–0.6 MPa. (C) Maximum depth at which cracking may occur in ice wedges for two possible tension thresholds (0.5 and 0.4 MPa) as a function of average winter ground surface temperatures of −38°C, −28°C, −18°C, and −8°C.

snow patches were also collected in well-sealed Ziploc bags, melted, and transferred to 20 ml HDPE bottles. All samples were shipped to the University of Ottawa for analyses.

Laboratory analyses

In the laboratory, the ice wedge samples were first melted in prebaked 500 mL glass beakers covered with plastic wrap and sealed to ensure no evaporation. Samples were then filtered in prerinsed 0.45 µm cellulose nitrate filters, with subsamples transferred in 20 mL plastic vials for major ions and δD-$\delta^{18}O$ analyses, in 40 ml amber glass vials for DOC and $\delta^{13}C_{DOC}$ analyses, and in prebaked 1 L glass amber bottles for $^{14}C_{DOC}$ analyses. The total water-soluble ions in the active layer were determined in the laboratory from sequential extractions of dried soils (<2 mm fraction) using a 1:10 soil:water ratio (e.g., Conklin, 2005). The soil–water mixtures were shaken for 1 h at room temperature and subsequently centrifuged and filtered with 0.45 µm prerinsed cellulose nitrate filters and stored in 40 ml amber glass vials until analysis for major ions, DOC, and $\delta^{13}C_{DOC}$.

Major cations and anions were analyzed in the Geochemical Laboratories at the University of Ottawa. The cations (Ca^{2+}, Mg^{2+}, Na^{+}, and K^{+}) were acidified with ultrapure nitric acid using an Agilent 4100 Microwave Plasma Emission Spectrometer. The anions (Cl^{-}, SO_4^{2-}, and NO_3^{-}) were analyzed unacidified by ion chromatography using a Dionex ICS-2100. Analytical precision is ±5%. To facilitate a comparison between ice wedges and leached active layer samples, the DOC results were converted to molar ratios with respect to Cl^{-}, a conservative tracer.

The source of moisture forming the ice wedge was inferred from δD-$\delta^{18}O$ analysis. The $^{18}O/^{16}O$ and D/H ratios of the melted ice wedges and residual snow were determined using a Los Gatos Research liquid water analyzer coupled with a CTC LC-PAL autosampler and verified for spectral interference contamination (Berman et al., 2009). The results are presented using the δ-notation, where δ represents the parts per thousand differences for $^{18}O/^{16}O$ or D/H in a sample with respect to Vienna Standard Mean Ocean Water. Analytical precision for $\delta^{18}O$ and δD was ±0.3‰ and ±1‰, respectively.

The source of DOC in the ice wedges was inferred from DOC (DOC/Cl) and $\delta^{13}C_{DOC}$ of melted ice wedge, residual snow, and leached active layer water. The [DOC] and $\delta^{13}C_{DOC}$ were measured by a wet total organic carbon (TOC) analyzer interfaced to a Thermo DeltaPlus XP isotope-ratio mass spectrometer at the Ján Veizer Stable Isotope Laboratory, University of Ottawa (St-Jean, 2003). The $^{13}C/^{12}C$ results are presented using the δ-notation relative to Vienna Pee Dee Belemnite. The analytical precision is ±0.5 ppm for DOC and ±0.2‰ for $\delta^{13}C_{TOC}$.

Radiocarbon analysis of the DOC of the ice wedges was performed at the A.E. Lalonde Accelerator Mass Spectrometry Laboratory, University of Ottawa. Sample preparation, including the extraction of DOC from waters and graphitization for ^{14}C analysis, is described in Murseli et al. (2019). Graphitized samples were analyzed on a 3MV tandem mass spectrometer (Kieser et al. 2015). The $^{14}C/^{12}C$ ratios are expressed as fraction of Modern Carbon ($F^{14}C$) and corrected for spectrometer and preparation fractionation using the $^{13}C/^{12}C$ ratio measured using accelerator mass spectrometry (Crann et al. 2017). Radiocarbon ages are calculated as $-8033\ln(F^{14}C)$ and reported in ^{14}C yr BP (BP = AD 1950) (Stuiver and Polach, 1977). The measurements were then converted to calendar years (cal yr BP) using OxCal v. 4.2.4 and the IntCal13 calibration curve (Bronk Ramsey, 2009; Reimer et al., 2013). In the text, radiocarbon ages with a standard error between 50 and 1000 yr are rounded to the nearest 10 yr.

https://doi.org/10.1017/qua.2020.126 Published online by Cambridge University Press

Table 1. $\delta^{18}O$, D-excess (*d*), and major ion (Ca^{2+}, Mg^{+}, Na^{+}, Cl^{-}, SO_4^{2-}) results for ice wedge samples at five sites in the Eureka Sound Lowlands, high Arctic Canada.[a]

Wedge no.	Distance from center (m)	$\delta^{18}O$ (‰)	*d* (‰)	Ca^{2+} (mg/L)	Mg^{+} (mg/L)	Na^{+} (mg/L)	Cl^{-} (mg/L)	SO_4^{2-} (mg/L)
Dump slump								
EU19-W1	0	−30.6	2.4	22.2	11.1	28.3	14.7	77.2
	1.6	−33.6	6.5	16.7	7.1	43.2	51.3	46.0
	−1.25	−29.1	3.6	13.0	7.3	78.7	70.6	54.5
	0.7	−32.5	6.1	19.3	8.5	58.9	56.8	83.4
	−0.65	−31.4	2.8	16.2	4.6	66.9	29.9	127.0
DS-W2	—	−35.1	12.3	5.9	2.0	9.6	13.6	10.2
Blacktop slump								
EU19-W2	−0.39	−27.6	−0.8	31.9	10.1	47.8	104.1	59.4
	0	−29.9	5.3	19.5	8.2	15.5	41.8	27.1
	0.45	−29.2	2.8	28.5	10.0	307.3	426.6	63.2
BT-W1	C	−31.6	13.4	10.1	4.0	15.1	23.4	20.2
	E	−31.7	13.6	13.0	3.5	13.3	20.3	24.5
BT-W2	E	−30.9	12.7	13.9	5.1	42.7	49.9	18.1
	C	n/d	n/d	14.9	5.4	45.6	53.5	18.8
Nunavut slump								
EU19-W3	0	−32.1	7.6	15.2	2.9	13.9	13.8	32.3
	0.3	−31.7	7.3	14.9	3.9	15.0	14.7	39.2
EU19-W4	−2.04	−30.3	0.9	14.2	3.5	9.8	12.5	29.2
	1.68	−32.5	6.4	9.0	4.5	20.4	19.5	29.2
EU19-W5	0.15	−30.4	6.5	9.1	2.7	16.8	19.4	26.5
	−0.15	−28.3	−2.0	6.5	3.0	17.6	11.6	17.1
	0	−30.6	5.3	8.7	5.4	38.8	33.0	44.5
Mokka Fjord slump								
MF1-W1	0	−31.7	6.8	10.6	2.3	11.9	15.1	25.2
	1.55	−30.8	5.1	16.4	1.9	9.5	12.5	29.9
	−1	−28.9	3.8	53.3	36.6	100.0	259.9	36.0
MF1-W2	0	−30.6	3.7	40.2	21.7	87.8	82.0	232.7
MF1-W3	1.5	−29.7	2.7	5.4	2.6	11.0	16.0	21.0
	−1.5	−29.5	3.6	10.5	5.0	25.2	31.2	38.8
MF-W1	C	n/d	n/d	16.2	4.8	6.5	8.4	6.1
MF-W2	C	n/d	n/d	n/d	n/d	n/d	n/d	n/d
	E	−30.8	12.1	10.7	3.4	14.7	11.6	38.2
Gemini slump								
Gem-W1	E	n/d	n/d	13.3	6.1	12.1	14.6	6.8
Gem-W2	C	n/d	n/d	13.9	5.8	11.3	13.1	6.7
	E	−28.7	5.7	10.3	4.2	11.0	13.0	4.4

[a]Distances from the centers of sampled ice wedges are provided when measurements were made; otherwise, they are indicated relative to the center (C) or edge (E) of the wedge. n/d, no data.

RESULTS

Winter temperatures and cracking of ice wedges

At Eureka, the 1980–2016 winter air temperature was −38.5 ± 1.7°C, with late winter snow depths of 14.9 ± 6.3 cm. The freezing *n*-factor (ratio of winter temperature at the ground surface to that in the air) for these conditions would be about 0.85 (see Riseborough and Smith, 1998), which would give a winter ground surface temperature of about −33°C. The resulting stress field following rapid cooling of a ground surface with a temperature of

https://doi.org/10.1017/qua.2020.126 Published online by Cambridge University Press

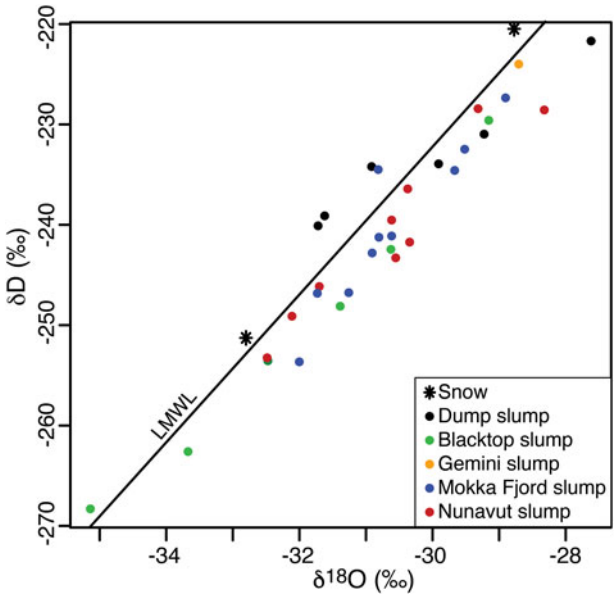

Fig. 3. (color online) δD-δ^{18}O composition of ice wedges sampled at five sites in the Eureka Sound Lowlands, high Arctic Canada. Also shown is the composition of two snow samples and the Eureka local meteoric water line (LMWL: δD = 7.4 δ^{18}O – 9.1; IAEA/WMO, 2015).

−33°C can generate cracks to a depth of 3.1–3.6 m, which is the depth where tension exceeds 0.4–0.5 MPa (Fig. 2). In the early Holocene, the winter air temperature was ca. 6−8°C warmer than today, and assuming a thicker snowpack (30–50 cm, corresponding to freezing *n*-factor of 0.65 to 0.5; Riseborough and Smith, 1998), winter ground surface temperatures could reach about −18°C. For this ground surface temperature, cracking depths would be in the 2.7 to 3.2 m range. These simulated cracking depths in ice wedges appear reasonable, as they are within the range of measured ice wedge depths in the region (average of 3.23 ± 0.8 m; Couture and Pollard, 1998). The simulations also predict little to no cracking at winter ground surface temperatures > −10°C, as reported in the literature, because the icy permafrost is less brittle and can respond by creep and elastic strain, so tension is poorly developed (see Mackay, 1993; Fortier and Allard, 2005). In the ESL, winter ground temperatures > −10°C could be reached if snow depth exceeds 1 m (corresponding to freezing *n*-factors in the 0.4 to 0.3 range; Riseborough and Smith, 1998).

Isotope chemistry of ice wedges and active layer

At Dump slump (33–36 m asl), three ice wedges were sampled. The δ^{18}O values in the six cores ranged from −35.1‰ to −29.2‰ (Table 1). The value of the regression slope between δD-δ^{18}O was 6.5 (δD = 6.5 δ^{18}O – 42.3; r^2 = 0.98), which is lower than the Eureka local meteoric water line (LMWL: δD = 7.4 δ^{18}O – 9.1; IAEA/WMO, 2015; Fig. 3). The three ice wedges had similar geochemical composition. The concentration of major cations averaged 15.0 ± 5.2 mg/L, 6.2 ± 3.1 mg/L, and 42.7 ± 26.7 mg/L for Ca^{2+}, Mg^{2+}, and Na^{+}, respectively; major anions averaged 36.6 ± 22.7 mg/L and 60.4 ± 39.3 mg/L for Cl^{-} and SO_4^{2-}, respectively (Table 1). The [DOC] averaged 1.0 ± 0.8 mg/L, with an average $\delta^{13}C_{DOC}$ of −25.7 ± 1.2‰. The DOC/Cl molar ratios in the ice wedges (0.16 ± 0.14) are similar to that of snow (1.5); the DOC/Cl in the active layer is much higher (5.55 ± 2.37) (Fig. 4). The $^{14}C_{DOC}$ ages of the ice wedges range from 28,950 to 12,130 cal yr BP, and the age in the center was older relative to the edges (Table 2). A $^{14}C_{DOC}$ age of 15,170 cal yr BP was obtained from the surrounding body of massive ice.

At Mokka Fjord slump (55–58 m asl), five ice wedges were sampled. The δ^{18}O values in the 10 cores ranged from −31.9‰ to −28.9‰ (Table 1). The value of the regression slope between δD-δ^{18}O was 7.5 (δD = 7.5 δ^{18}O – 9.6; r^2 = 0.87), which is close to the Eureka LMWL (Fig. 3). All three wedges had similar geochemical composition. The concentration of major cations averaged 14.3 ± 9.6 mg/L, 5.7 ± 5.8 mg/L, and 22.8 ± 23.7 mg/L for Ca^{2+}, Mg^{2+}, and Na^{+}, respectively; major anions averaged 27.6 ± 21.8 mg/L and 47.6 ± 65.8 mg/L for Cl^{-} and SO_4^{2-}, respectively (Table 1). The [DOC] averaged 8.4 ± 15.1 mg/L, with $\delta^{13}C_{DOC}$ averaging −25.9 ± 0.5‰. The DOC/Cl ratios in the ice wedges (0.31 ± 0.26) are similar to that of snow; the DOC/Cl in the active layer is higher (13.44 ± 9.58) (Fig. 4). The five ice wedges were analyzed for $^{14}C_{DOC}$; the ages ranged from 8100 to 2586 cal yr BP, and the $^{14}C_{DOC}$ age was younger in the center relative to the edges (Table 2).

At Blacktop slump (60–66 m asl), three ice wedges were sampled. The δ^{18}O values in the seven cores ranged from −31.7‰ to −27.6‰ (Table 1). The value of the regression slope between δD-δ^{18}O was 4.1 (δD = 4.1 δ^{18}O – 108.5; r^2 = 0.95), which is lower than the Eureka LMWL (Fig. 3). The concentration of major cations averaged 18.8 ± 8.3 mg/L, 6.6 ± 2.7 mg/L, and 69.6 ± 105.9 mg/L for Ca^{2+}, Mg^{2+}, and Na^{+}, respectively; major anions averaged 102.8 ± 145.4 mg/L and 33.1 ± 19.6 mg/L for Cl^{-} and SO_4^{2-}, respectively (Table 1). The [DOC] averaged 5.5 ± 2.9 mg/L, with the $\delta^{13}C_{DOC}$ averaging −24.5 ± 0.1‰. The ice wedges have DOC/Cl (0.16 ± 0.13) ratios similar to that of snow; the DOC/Cl in the active layer is higher (5.76 ± 3.91) (Fig. 4). The $^{14}C_{DOC}$ of the ice wedges ranged from 33,130 to 5998 cal yr BP and the ice was younger in the center relative to the edges (Table 2).

At Nunavut slump (73–100 m asl), three ice wedges were sampled. The δ^{18}O values in the nine cores ranged from −32.4‰ to −28.3‰ (Table 1). The value of the regression slope between δD-δ^{18}O was 6.2 (δD = 6.2 δ^{18}O – 50.7; r^2 = 0.91), which is lower than the Eureka LMWL (Fig. 3). All three wedges had similar geochemical composition (Fig. 4). The concentration of major cations averaged 11.9 ± 6.4 mg/L, 4.7 ± 3.2 mg/L, and 21.9 ± 14.7 mg/L for Ca^{2+}, Mg^{2+}, and Na^{+}, respectively; major anions averaged 20.9 ± 14.7 mg/L and 34.4 ± 21.1 mg/L for Cl^{-} and SO_4^{2-}, respectively (Table 1). The [DOC] averaged 3.6 ± 1.5 mg/L, with the $\delta^{13}C_{DOC}$ averaging −25.1 ± 0.5‰. The ice wedges have DOC/Cl (0.72 ± 0.60) ratios similar to that of snow; the DOC/Cl in the active layer is higher (12.61 ± 11.90) (Fig. 4). The $^{14}C_{DOC}$ of the three ice wedges ranged from 8100 to 6885 cal yr BP, and with the exception of EU19-W5, a younger age was obtained in the center relative to the edges (Table 2).

At the Gemini site (120 m asl), two ice wedges were sampled. The δ^{18}O was measured in one sample only and yielded a value of −28.7‰ (Fig. 3). The concentration of major cations in the two wedges averaged 12.5 ± 1.9 mg/L, 5.4 ± 0.9 mg/L, and 11.5 ± 0.6 mg/L for Ca^{2+}, Mg^{2+}, and Na^{+}, respectively; major anions averaged 13.5 ± 0.9 mg/L and 5.9 ± 1.3 mg/L for Cl^{-} and SO_4^{2-}, respectively (Table 1). The [DOC] averaged 4.9 ± 1.5 mg/L. The two ice wedges have DOC/Cl (1.07 ± 0.26) ratios similar to that of snow; the active layer was not sampled at this site (Fig. 4). The $^{14}C_{DOC}$ of the two ice wedges ranged from 5412 to 2753 cal yr BP, and the younger age was obtained in the center relative to the edges (Table 2).

https://doi.org/10.1017/qua.2020.126 Published online by Cambridge University Press

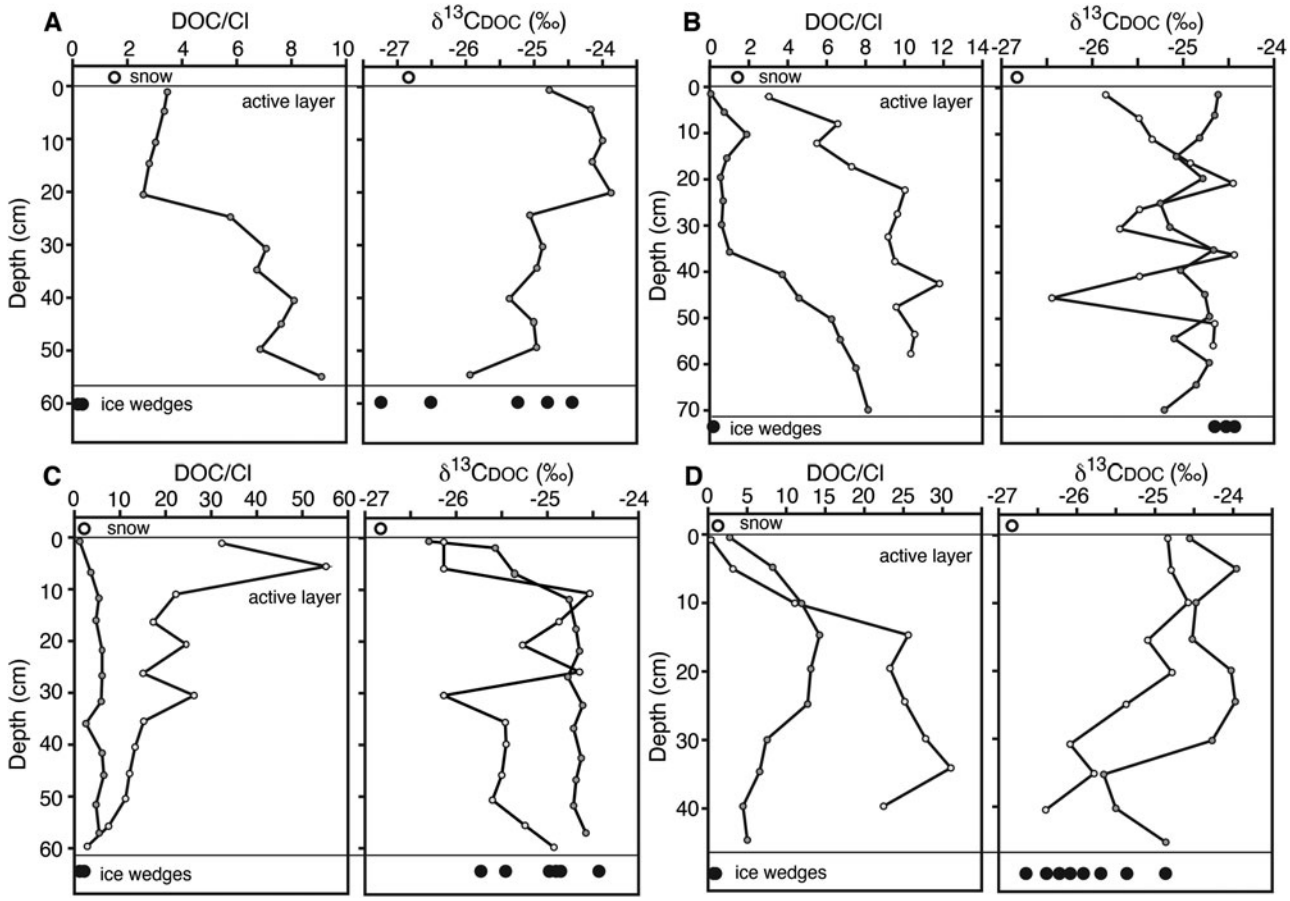

Fig. 4. (color online) Dissolved organic carbon (DOC)/Cl (molar ratio) and $\delta^{13}C_{DOC}$ composition in the ice wedges, snow, and leached active layer at four sites in the Eureka Sound Lowlands, high Arctic Canada. (A) Dump slump, (B) Blacktop slump, (C) Nunavut slump, (D) Mokka slump.

DISCUSSION

Source of moisture and DOC in the ice wedges

On the Fosheim Peninsula, the glacial and marine sediments contain reworked Tertiary material, including carbon, that could yield older ^{14}C ages if it leached into DOC. The source of DOC in the ice wedges was first assessed from δD-$\delta^{18}O$ and DOC/Cl before the $^{14}C_{DOC}$ measurements were used to infer the timing of ice wedge formation. Once a crack forms in winter, it can be infilled by one or more sources of moisture: (1) snow, (2) hoarfrost accretion, and (3) snow meltwater (Mackay, 1992; Lauriol et al., 1995; St-Jean et al., 2011; Boereboom et al., 2013). The $\delta^{18}O$ composition of the ice wedges ranges from −35.1‰ to −27.6‰, which is in the range of the two sampled residual snow patches (Fig. 3). The δD-$\delta^{18}O$ composition of the ice wedges is distributed along a regression slope value of 6.6 ($\delta D = 6.6\ \delta^{18}O - 37.8$; $r^2 = 0.91$), which is lower than the LWML (7.4) and suggests ice wedges developed from the freezing of snow meltwater that infiltrated the cracks (see Lacelle, 2011).

For ice wedges forming from the freezing of snowmelt, the DOC in the wedges originates from the snowmelt, but additional DOC may be leached from the active layer as the meltwater infiltrates the cracks. The [DOC] of the ice wedges in the ESL averaged 3.3 ± 1.7 mg/L (0.88 to 8.7 mg/L), which is within the range of the snow sample (2.1 mg/L) and concentrations measured in ice wedges on Hershel Island (Yukon Territory, Canada) (2.4 to 8.8 mg/L; Tanski et al., 2016), in central Yukon Territory (8.1 to 16.3 mg/L; Grinter et al., 2019), and in Alaska (USA) and Siberia (Russia) (1.6 to 28.6 mg/L; Fritz et al., 2015). Considering that the concentration of solutes can increase during freezing, the DOC/Cl molar ratio was used to assess the source of DOC in the ice wedges. At the five sites, the DOC/Cl ratios of the ice wedges (0.36 ± 0.29) are closer to that of the snow (1.5) but are significantly lower than in the leached active layer samples (8.87 ± 8.59; two-tailed *t*-test, $P < 0.05$) (Fig. 4). The $\delta^{13}C_{DOC}$ cannot distinguish between the source of the DOC in the ice wedges (−25.4 ± 0.8‰), as it is within the range of both the snow (−26.8‰) and the leached active layer (−24.9 ± 0.6‰). Therefore, the DOC/Cl suggests that the DOC in the ice wedges is sourced from the snowmelt and not leached from the active layer, which can release Tertiary-age organics contained in the frozen marine sediments. Although the $^{14}C_{DOC}$ of snow meltwater was not measured, it is assumed to have a modern DOC signature at the time of infiltration. For example, Grinter et al. (2019) showed that snow meltwater and spring freshets of the Ogilvie River in central Yukon had similar [DOC], both with modern $^{14}C_{DOC}$ ages.

Cracking probability, width, and period of growth of ice wedges

Epigenetic ice wedges, such as those sampled in the ESL, develop in pre-existing permafrost and grow progressively wider from the center of the wedge (Mackay, 1990). The ice wedges in this study

https://doi.org/10.1017/qua.2020.126 Published online by Cambridge University Press

Table 2. Dissolved organic carbon (DOC), $\delta^{13}C_{DOC}$, and $^{14}C_{DOC}$ results for ice wedges sampled at five sites in Eureka Sound Lowlands, high Arctic Canada.[a]

Wedge no.	Distance from center (m)	DOC (ppm)	$\delta^{13}C_{DOC}$ (‰)	^{14}C yr BP	(±2σ)	$F^{14}C$	±2σ	Median cal yr BP	Lab ID
Dump slump									
EU19-W1	0	0.96	−24.5	22,146	163	0.0635	0.0013	26,370	UOC-11064
	1.6	1.26	−25.3	13,636	69	0.1832	0.0016	16,437	UOC-11065
	−1.25	2.92	−26.5	24,872	367	0.0452	0.0021	28,954	UOC-11066
	0.7	1.48	−24.9	14,480	109	0.1649	0.0022	17,651	UOC-11067
	−0.65	0.88	−27.2	10,308	75	0.2772	0.0026	12,125	UOC-11068
DS-W2		2.0	n/d	14,641	64	0.1616	0.0013	17,823	UOC-6087
Blacktop slump									
EU19-W2	−0.39	4.67	−24.4	9883	45	0.2922	0.0017	11,278	UOC-12524
	0	3.13	−24.6	6320	36	0.4553	0.002	7250	UOC-12525
	0.45	8.68	−24.5	12,127	61	0.221	0.0017	13,994	UOC-12526
BT-W1	C	2.8	n/d	5251	30	0.5201	0.0020	5998	UOC-6082
	E	2.0	n/d	6480	38	0.4463	0.0021	7381	UOC-6088
BT-W2	E	2.8	n/d	22,043	117	0.0643	0.0009	26,249	UOC-6084
	C	2.5	n/d	28,948	269	0.0272	0.0009	33,131	UOC-6080
Nunavut slump									
EU19-W3	0	1.88	−25.4	6038	41	0.4716	0.0024	6885	UOC-11070
	0.3	2.71	−25.0	7088	39	0.4138	0.002	7919	UOC-12527
EU19-W4	−2.04	2.30	−25.7	7288	39	0.4036	0.002	8100	UOC-12528
	1.68	3.94	−24.8	6251	42	0.4593	0.0024	7190	UOC-11071
EU19-W5	0.15	2.06	−25.7	6614	36	0.439	0.002	7506	UOC-12529
	−0.15	5.61	−24.4	7739	35	0.3816	0.0016	8514	UOC-12530
	0	4.59	−24.9	7222	37	0.407	0.0019	8028	UOC-11072
Mokka Fjord slump									
MF1-W1	0	2.56	−26.1	2503	33	0.7323	0.003	2587	UOC-12531
	1.55	2.78	−26.7	3438	35	0.6518	0.0028	3694	UOC-11073
	−1	48.6	−24.9	6061	48	0.4703	0.0028	6917	UOC-12532
MF1-W2	0	3.25	−25.4	4347	44	0.5821	0.0032	4921	UOC-12533
MF1-W3	1.5	3.20	−26.2	5941	36	0.4773	0.0022	6765	UOC-12534
	−1.5	3.86	−25.7	7077	58	0.4144	0.0030	7900	UOC-12535
MF-W1	C	n/d	n/d	7296	47	0.4032	0.0024	8102	UOC-6083
MF-W2	C	n/d	n/d	3047	29	0.6843	0.0025	3256	UOC-6085
	E	n/d	n/d	5237	34	0.5210	0.0022	5981	UOC-6089
Gemini slump									
Gem-W1	E	6.7	n/d	2624	28	0.7213	0.0025	2753	UOC-6081
Gem-W2	C	4.4	n/d	2980	29	0.6900	0.0025	3153	UOC-6090
	E	3.7	n/d	4619	29	0.5627	0.0020	5312	UOC-6086

[a]Distances from center of ice wedges are provided when measurements were made, otherwise, they are indicated relative to center (C) or edge (E) of the wedge. n/d, no data.

yielded younger $^{14}C_{DOC}$ ages near the center with older ages near the edges, and positive relationships were observed between their widths and ranges of $^{14}C_{DOC}$ ages (Table 2). However, while one can count layers to establish a robust chronology for glaciers, the same cannot be done with individual veins forming the ice wedges. The frequency of ice wedge cracking is variable and depends primarily on winter air and ground temperatures, the latter being dependent on snow depth, vegetation cover, and polygon morphology (Mackay, 1992, 1993; Fortier and Allard, 2005; Abolt et al., 2018).

https://doi.org/10.1017/qua.2020.126 Published online by Cambridge University Press

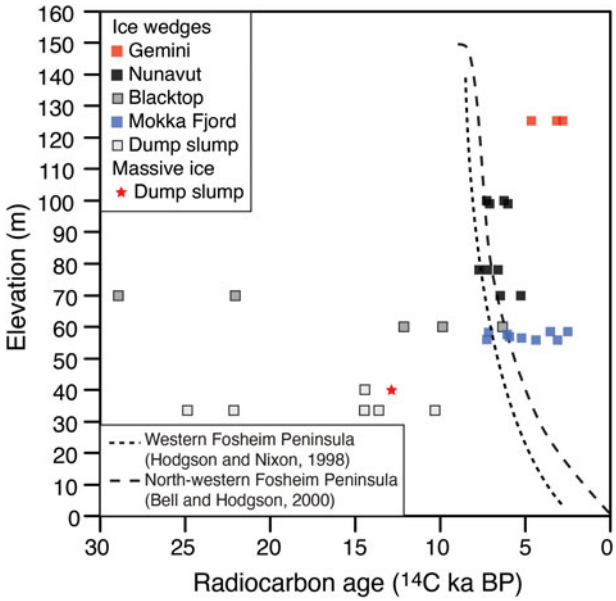

Fig. 5. (color online) Comparison of radiocarbon dating of dissolved organic carbon ($^{14}C_{DOC}$) of ice wedges sampled at different elevation with the regional isostatic curves. Marine regression curves are from Hodgson and Nixon (1998) and Bell and Hodgson (2000).

Based on measurements from Garry Island (Mackenzie Delta region, Northwest Territories, Canada), Mackay (1974) suggested that the probability of cracking (P) of ice wedges follows a Gaussian distribution and can be estimated from the average width (μ) and standard deviation (σ) of a population of ice wedges:

$$P = \frac{1}{\sigma\sqrt{2\pi}} e^{\frac{-(x-\mu)^2}{2\sigma^2}} \quad \text{(Eq. 1)}$$

This equation can then be combined with the annual ice wedge growth increment (ΔX, typically 1–5 mm) to estimate the number of years (T_{ji}) required to increase the width from X_i to X_j:

$$T_{ji} = \frac{(X_j - X_i)}{\Delta X P_{ij}} \quad \text{(Eq. 2)}$$

where, P_{ji} is the mean probability of cracking for that growth interval.

The time period of ice wedge growth of width A_j, can then be estimated from Eq. 3 and compared with our measurements of $^{14}C_{DOC}$ and width for the ice wedges:

$$A_j = \Sigma T_{j1} \text{ for the period of 1 to } j \quad \text{(Eq. 3)}$$

A cracking probability curve was established for ice wedges in the ESL using the average widths of 1.46 ± 0.56 m (n = 150; Couture and Pollard, 1998), and the estimated age curve was then established using three possible growth increments (2, 2.5, and 3 mm) that are within the range of that reported by Lewkowicz (1994). The widths and $^{14}C_{DOC}$ age ranges of the sampled ice wedges from the different sites show a good fit with the theoretical age distribution curve as a function of ice wedge width using the 2–2.5 mm growth increment, especially considering the sensitivity of the age curve to the cracking probability (an improved fit is obtained using an average width of 1.36 m instead of 1.46 m; Fig. 5). The good fit between the widths of ice wedges and $^{14}C_{DOC}$ age range appears to validate the concept of cracking probability, width, and growth period proposed by Mackay (1974) and suggests that the age of ice wedges cannot simply be determined by interpolating between measurements, as the cracking frequency is modified as the wedge grows.

Paleo-geography and development of ice wedges in the ESL

The latest glacial reconstruction suggests that the ESL was glaciated by the Innuitian Ice Sheet and deglaciation started between 10,300 and 8800 ^{14}C yr BP (England et al., 2006). Marine transgression occurred until 8800–7800 ^{14}C yr BP with the Holocene marine limit near Eureka reaching 146 m asl (Bell, 1996). The $^{14}C_{DOC}$ ages obtained from ice wedges across elevations of 120 to 33 m asl are compared with the local marine emergence curves

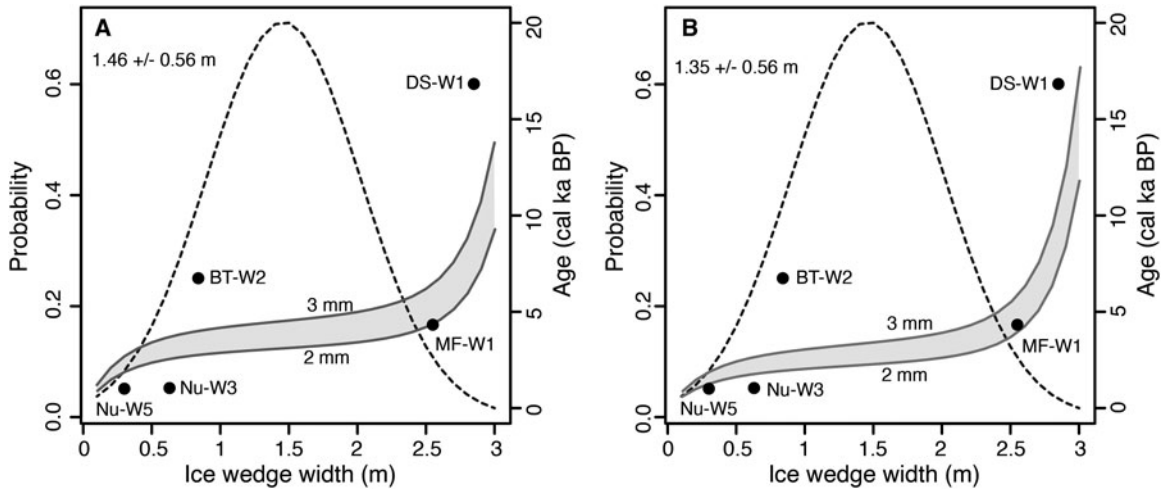

Fig. 6. Probability of ice wedge cracking and age–width relation in ice wedges in the Eureka Sound Lowlands, high Arctic Canada. Dashed line represents the probability of ice wedge cracking, which is assumed to follow a Gaussian distribution for (A) a mean of 1.46 and standard deviation of 0.56 m and (B) a mean of 1.36 and standard deviation of 0.56 m (see Eq. 1). Envelope represents the theoretical widths and ages of ice wedges for growth increments of 2 to 3 mm (see Eqs. 2 and 3). Dots represents the measured width and radiocarbon dating of dissolved organic carbon ($^{14}C_{DOC}$) age range in ice wedges in the Eureka Sound Lowlands.

https://doi.org/10.1017/qua.2020.126 Published online by Cambridge University Press

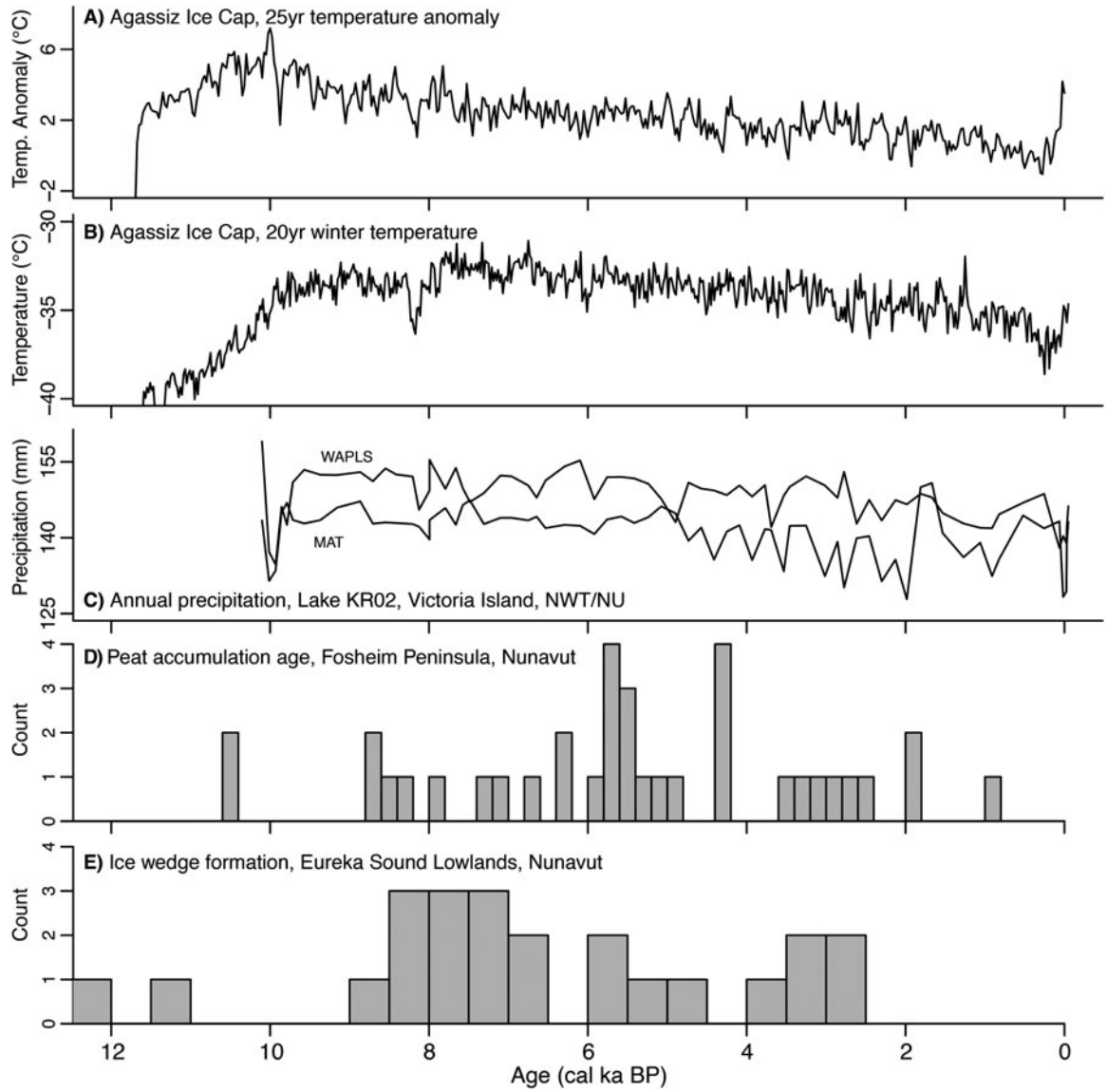

Fig. 7. Frequency distribution of ice wedge activity in the Eureka Sound Lowlands, high Arctic Canada, compared with various paleoclimate proxies. (A) 25-yr mean annual temperature anomaly derived from Agassiz Ice Cap $\delta^{18}O$ record (Lecavalier et al., 2017); (B) 20-yr mean winter air temperature derived from Agassiz Ice Cap $\delta^{18}O$ record (Buizert et al., 2018); (C) annual precipitation reconstruction from a pollen record on Victoria Island (Peros and Gajewski, 2008). The two curves are derived from distinct climate transfer functions. MAT, modern analogue technique; WAPLS, weighted averaging partial least squares. Distribution of peat accumulation age on the Fosheim Peninsula (Garneau, 2000); (E) radiocarbon dating of dissolved organic carbon ($^{14}C_{DOC}$) age distribution from ice wedges in the Eureka Sound Lowlands.

(Fig. 6). The majority of the $^{14}C_{DOC}$ ages of the ice wedges sampled at Gemini, Nunavut, and Mokka Fjord slumps fall along or above the marine regression curves. This suggests that, at these sites, conditions became suitable for the aggradation of permafrost and subsequent ice wedge development in the marine sediments occurred immediately or shortly after permafrost aggradation. This is analogous to contemporary studies that observed the development of ice wedges in recently drained lake beds, for example, at the Illisarvik drained-lake basin in the Mackenzie Delta (Mackay, 2000).

The $^{14}C_{DOC}$ ages of ice wedges at Blacktop slump (28,950 to 5251 ^{14}C yr BP) and Dump slump (24,870 to 10,310 ^{14}C yr BP), both situated closest to the coast, are distributed below the marine regression curves. This was an unexpected finding, either at these sites: (1) ice wedges were developing in an ice-free region during the last glaciation (see England, 1987; Lemmen, 1989); (2) the $^{14}C_{DOC}$ ages were contaminated with Tertiary organic material; or (3) these ice wedges formed from a mixture of late Pleistocene–age glacial meltwater and snow meltwater. The development of ice wedges in an ice-free region can be ruled out because the wedges at Dump slump developed in massive ice with DOC dated to 12,730 ^{14}C yr BP (similar to the age obtained in the ice wedges; Table 1), whereas those at Blacktop slump developed in Holocene-age ice-rich marine sediments. A contamination from Tertiary-age organic material can also be ruled out as the DOC/Cl ratios of the ice wedges do not support the leaching of DOC from the frozen active layer. The most likely explanation is that these ice wedges formed from a mixture of late Pleistocene–age glacial meltwater and snow meltwater, with the glacial meltwater providing the majority of the source water.

https://doi.org/10.1017/qua.2020.126 Published online by Cambridge University Press

Support for this hypothesis comes from the lower $\delta^{18}O$ composition of these ice wedges (−33.6‰ to −29.1‰; Fig. 3), and their [DOC] and major ions (DOC: 2.7 ± 3.0 mg/L; Ca^{2+}: 19.3 ± 5.4 mg/L; Mg^{2+}: 8.1 ± 2.3 mg/L; Na^{+}: 97.2 ± 104.4 mg/L; Cl^{-}: 108.3 ± 157.2 mg/L; SO_4^{2-}: 75.2 ± 28.9 mg/L), which are slightly higher relative to the other ice wedges but in the range of late Pleistocene glacial ice at Penny Ice Cap (Fisher et al., 1998). The landscape following deglaciation was vastly different from today. The ice wedges at Blacktop and Dump slumps could have developed shortly after marine regression (ca. 6000 ^{14}C yr BP for the 30–70 m elevation range), with the water being sourced from the melting of residual ice caps remaining on top of Blacktop Ridge or other nearby locations (see Bell, 1992).

Holocene ice wedge activity in the ESL

The $^{14}C_{DOC}$ age distribution of ice wedges can be used as proxies for paleoenvironmental conditions, because their development requires: (1) the presence of icy permafrost; (2) mean winter air temperatures < −10°C; (3) surface conditions that allow cracking of the ice wedge when air temperatures rapidly decrease; and (4) a moisture source to fill the crack (Washburn 1980; Harry and Gozdzik 1988; Christiansen et al. 2016). Figure 7 compares the $^{14}C_{DOC}$ age distribution of ice wedges in the ESL with Holocene paleotemperature reconstructions from the nearby Agassiz Ice Cap (25-yr mean annual air temperature record [Lecavalier et al., 2017] and 20-yr mean winter air temperature record [Buizert et al., 2018]), Holocene precipitation reconstructions on Victoria Island that included modern analog sites from the Fosheim Peninsula (Peros and Gajewski, 2008), and the period of peat accumulation in the Fosheim Peninsula (Garneau, 2000). The $^{14}C_{DOC}$ ages, beyond having a degree of analytical and calibration uncertainties, represent a range in ages, as samples were collected across multiple ice veins using a core barrel with diameter of 8.8 cm and $^{14}C_{DOC}$ ages were grouped in 500 yr bins.

The distribution of the 32 $^{14}C_{DOC}$ ages of ice wedges in the ESL cluster in three periods of activity: (1) immediately to shortly after marine regression and subsequent permafrost aggradation in the marine sediments (9000–6500 cal yr BP), (2) between 6000 and 4500 cal yr BP, and (3) between 4000 and 2500 cal yr BP. However, given that the ice wedges were sampled at discrete locations and reported ages are not continuous across their width, it is likely the ice wedges were active over the 9000 to 2500 cal yr BP period (Fig. 7). The $^{14}C_{DOC}$ age distribution of ice wedges is very similar to the period of peat accumulation on the Fosheim Peninsula, where all sites with peat accumulation over 50 cm thick yielded ^{14}C ages between 8500 and 2500 cal yr BP (Garneau, 2000). The temperatures were likely always favorable to cracking and the growth of ice wedges (even if snow reached 1 m depth), considering that Holocene winter temperatures in the ESL reached a maximum of about −30°C (Fig. 2). However, in this polar desert environment, both the ice wedges and peatlands require sufficient moisture to develop. Reconstructed Holocene precipitation from Victoria Island suggests that precipitation during the early and mid-Holocene was 10%–15% higher than in the present day. The increased precipitation was attributed to the marine transgression and reduced sea ice cover, which imparted a stronger maritime influence on the climate (Koerner, 1977). A transition to a near present-day level of precipitation occurred near the onset of the late Holocene (4200 cal yr BP) with the cooler and drier conditions lasting through the Little Ice Age (Peros and Gajewski, 2008). Therefore, the transition to the drier climate conditions near the start of the late Holocene corresponds to the reduced ice wedge formation and peat accumulation, as an insufficient amount of moisture was present to allow for their development. An estimate of the volume of snow meltwater required to fill a crack in an ice wedge can be made with knowledge on crack geometry and snow depth. Approximately 4.5–5 L of snow meltwater is required to fill a 3- to 3.5-m-deep crack over a 1 m section with an ~3-mm-wide vein. For the average width of polygonal troughs in the ESL (1.46 ± 0.56 m), sufficient meltwater is provided if the snow depth is about 30 cm. This calculation assumes that the snow meltwater is sourced directly from the trough above the crack and ignores the fact that snowmelt may also originate from the center of polygons or from nearby hillslopes. However, it does suggest that snow depth <30 cm may not provide sufficient meltwater to fill a 3- to 3.5-m-deep crack. The 1980–2016 snow depths at Eureka are near that threshold, with late winter snow depth ranging between 5 and 35 cm (Environment Canada, 2019). The observed rejuvenation of certain ice wedges in the ESL (see Lewkowicz, 1994) could be associated with the increase in precipitation over the past few years (e.g., Copland et al., 2020). Therefore, the relationship between current ice wedge formation and snow conditions is likely symbiotic, with the distribution of snow affecting the ground thermal regime and the formation of ice wedge troughs affecting the snow distribution and moisture sources.

CONCLUSION

This study investigated the timing of formation of ice wedges in the ESL, a high Arctic polar desert environment. Based on the results, five conclusions can be made.

First, simulations of stress induced in ice wedges following rapid cooling suggest that the cracking of ice wedges may occur when ground surface temperatures are < −10°C, with cracks to depths of 2.5 to 3.5 m. These results correspond well with the observed depths of epigenetic ice wedges in Eureka. Ice wedges observed at greater depths (>4 m) are likely of syngenetic origin and developed in colluviated sediment along hillslopes.

Second, the $\delta^{18}O$ composition, [DOC], and DOC/Cl molar ratios of the ice wedges match those of residual snow patches. This suggests that ice wedges developed from the freezing of snow meltwater, with the DOC sourced from snowmelt and not from the leaching of organics in the active layer.

Third, the majority of ice wedges had $^{14}C_{DOC}$ ages younger than the regional isostatic curves, suggesting that conditions became suitable for the aggradation of permafrost and subsequent ice wedge development in the marine sediments after marine regression.

Fourth, Mackay (1974) proposed a cracking probability model of ice wedges from which their growth periods could be estimated from their widths. The model was tested against the average widths of ice wedges in the ESL and three possible growth increments (2, 2.5, and 3 mm). A good fit was observed between the widths of ice wedges and $^{14}C_{DOC}$ age ranges, which supports the concept of cracking probability, width, and growth period proposed by Mackay (1974) and suggests that the age of ice wedges cannot simply be determined by interpolating between measurements.

Finally, the distribution of $^{14}C_{DOC}$ of ice wedges in the ESL follows closely that of regional peat accumulation, with ice wedge active mainly between 9000 and 2500 cal yr BP. Given that

https://doi.org/10.1017/qua.2020.126 Published online by Cambridge University Press

temperatures were always favorable to ice wedge growth, the corresponding periods of ice wedge activity and peat accumulation reflect increased precipitation.

Acknowledgments. We would like to thank C. Roy and B. Faucher for valuable field assistance and the staff at the Eureka Weather Station for accommodations. We thank T. Porter, an anonymous reviewer, and the editorial office (D. Booth and T. Lowell) for their constructive comments.

Financial support. This project was supported by a Natural Sciences and Engineering Research Council of Canada (NSERC) Discovery Grant, with logistical support provided by NSERC Northern Supplement, Polar Continental Shelf Project (project no. 653-19), and the Northern Scientific Training Program.

REFERENCES

Abolt, C.J., Young, M.H., Atchley, A.L., Harp, D.R., 2018. Microtopographic control on the ground thermal regime in ice wedge polygons. *Cryosphere* **12**, 1957–1968.

Becker, M.S., Davies, T.J., Pollard, W.H., 2016. Ground ice melt in the high Arctic leads to greater ecological heterogeneity. *Journal of Ecology* **104**, 114–124.

Bell, T., 1992. *Glacial and Sea Level History of Western Fosheim Peninsula, Ellesmere Island, Arctic Canada*. PhD thesis, University of Alberta, Edmonton, Canada.

Bell, T., 1996. The last glaciation and sea level history of Fosheim Peninsula. Ellesmere Island, Canadian High Arctic. *Canadian Journal of Earth Sciences* **33**, 1075–1086.

Bell, T., Hodgson, D.A., 2000. Quaternary geology and glacial history of Fosheim Peninsula, Ellesmere Island, Nanavut. In: Garneau, M., Alt, B.T. (Eds.), *Environmental Response to Climate Change in the Canadian High Arctic. Geological Survey of Canada Bulletin* 529, 175–196.

Berman, E.S.F., Gupta, M., Gabrielli, C., Garland, T., McDonnell, J.J., 2009. High-frequency field-deployable isotope analyzer for hydrological applications. *Water Resources Research* **45**. http://dx.doi.org/10.1029/2009WR008265.

Bernard-Grand'Maison, C., Pollard, W., 2018. An estimate of ice wedge volume for a High Arctic polar desert environment, Fosheim Peninsula, Ellesmere Island. *Cryosphere* **12**, 3589–3604.

Boereboom, T., Samyn, D., Meyer, H., Tison, J.-L., 2013. Stable isotope and gas properties of two climatically contrasting (Pleistocene and Holocene) ice wedges from Cape Mamontov Klyk, Laptev Sea, northern Siberia. *Cryosphere* **7**, 31–46.

Bronk Ramsey, C., 2009. Bayesian analysis of radiocarbon dates. *Radiocarbon* **51**, 337–360.

Buizert, C., Keisling, B.A., Box, J.E., He, F., Carlson, A.E., Sinclair, G., DeConto, R.M., 2018. Greenland-wide seasonal temperatures during the last deglaciation. *Geophysical Research Letters* **45**, 1905–1914.

Christiansen, H.H., Matsuoka, N., Watanabe, T., 2016. Progress in understanding the dynamics, internal structure and palaeoenvironmental potential of ice wedges and sand wedges. *Permafrost and Periglacial Processes* **27**, 365–376.

Conklin, A.R., Jr., 2005. *Introduction to Soil Chemistry: Analysis and Instrumentation*. Wiley, Hoboken, NJ.

Copland, L., Lacelle, D., Fisher, D., Delaney, F., Thomson, L., Main, B., Burgess, D., 2020. Warmer–wetter climate drives shift in δD–δ^{18}O composition of precipitation across the Queen Elizabeth Islands, Arctic Canada. *Arctic Science* (in press) https://doi.org/10.1139/as-2020-0009

Couture, N.J., Pollard, W.H., 1998. An assessment of ground ice volume near Eureka, Northwest Territories. In: Lewkowicz, A.G., Allard, M. (Eds.), Permafrost: Seventh International Conference. Yellowknife, Canada. Collection Nordicana No. 57, Pages 195–200.

Couture, N.J., Pollard, W.H., 2007. Modelling geomorphic response to climatic change. *Climate Change* **85**, 407–431.

Crann, C.A., Murseli, S., St-Jean, G., Zhao, X., Clark, I.D., Kieser, W.E., 2017. First status report on radiocarbon sample preparation techniques at the A.E. Lalonde AMS Laboratory (Ottawa, Canada). *Radiocarbon* **59**, 695–704.

Dyke, A.S., Andrews, J.T., Clark, P.U., England, J.H., Miller, G.H., Shaw, J., Veillette, J.J., 2002. The Laurentide and Innuitian ice sheets during the Last Glacial Maximum. *Quaternary Science Reviews* **21**, 9–31.

Edlund, S.A., Alt, B.T., 1989. Regional congruence of vegetation and summer climate patterns in the Queen Elizabeth Islands, Northwest Territories, Canada. *Arctic* **42**, 3–23.

Edlund, S.A., Alt, B.T., Garneau, M., 2000. Vegetation patterns on Fosheim Peninsula, Ellesmere Island, Nunavut. In: Garneau, M., Alt, B.T. (Eds.), *Environmental Response to Climate Change in the Canadian High Arctic. Geological Survey of Canada Bulletin* 529, 129–143.

England, J., 1987. Glaciation and the evolution of the Canadian high arctic landscape. *Geology* **15**, 419–424.

England, J., Atkinson, N., Bednarski, J., Dyke, A.S., Hodgson, D.A., Ó Cofaigh, C., 2006. The Innuitian ice sheet: configuration, dynamics and chronology. *Quaternary Science Reviews* **25**, 689–703.

Environment Canada 2019. Historical Canadian climate database. https://climate.weather.gc.ca/.

Fisher, D.A., 2005. A process to make massive ice in the Martian regolith using long-term diffusion and thermal cracking. *Icarus* **179**, 387–397.

Fisher, D.A., Koerner, R.M., Bourgeois, J.C., Zielinski, G., Wake, C., Hammer, C.U., Clausen, H.B., *et al.*, 1998. Penny Ice Cap cores, Baffin Island, Canada, and the Wisconsinan Foxe Dome connection: two states of Hudson Bay ice cover. *Science* **279**, 692–696.

Fisher, D.A., Lacelle, D., 2014. A model for co-isotopic signatures of evolving ground ice in the cold dry environments of Earth and Mars. *Icarus* **243**, 454–470.

Fisher, D.A., Lacelle, D., Pollard, W. 2020. A model of unfrozen water content and its transport in icy permafrost soils: effects on ground ice content and permafrost stability. *Permafrost and Periglacial Processes* **31**, 184–199. http://dx.doi.org/10.1002/ppp.2031.

Fortier, D., Allard, M. 2005. Frost-cracking conditions, Bylot Island, eastern Canadian Arctic archipelago. *Permafrost and Periglacial Processes* **16**, 145–161.

French, H.M., 2013. *The Periglacial Environment*. 3rd ed. Wiley, Hoboken, NJ.

French, H.M., Guglielmin, M., 2000. Frozen ground phenomena in the vicinity of the Terra Nova bay, Northern Victoria land, Antarctica: a preliminary report. *Geografiska Annaler Series A: Physical Geography* **82**, 513–526.

Fritz, M., Opel, T., Tanski, G., Herzschuh, U., Meyer, H., Eulenburg, A., Lantuit, H., 2015. Dissolved organic carbon (DOC) in Arctic ground ice. *Cryosphere* **9**, 737–752.

Garneau, M., 2000. Peat accumulation and climatic change in the High Arctic. In: Garneau, M., Alt, B.T. (Eds.), *Environmental Response to Climate Change in the Canadian High Arctic. Geological Survey of Canada Bulletin* 529, 283–293.

Grinter, M., Lacelle, D., Baranova, N., Murseli, S., Clark, I.D., 2019. Late Pleistocene and Holocene ice-wedge activity on the Blackstone Plateau, central Yukon, Canada. *Quaternary Research* **91**, 179–193.

Harry, D.G., Gozdzik, J.S., 1988. Ice wedges: growth, thaw transformation, and palaeoenvironmental significance. *Journal of Quaternary Science* **3**, 39–55. doi:10.1002/jqs.3390030107.

Hodgson, D.A., Nixon, F.M., 1998. *Ground Ice Volumes Determined from Shallow Cores from Western Fosheim Peninsula Ellesmere Island, Northwest Territories. Geological Survey of Canada Bulletin* 507. Government of Canada, Ottawa.

Holland, K.M., Porter, T.J., Froese, D.G., Kokelj, S.V., Buchanan, C.A., 2020. Ice-wedge evidence of Holocene winter warming in the Canadian Arctic. Geophysical Research Letters 47. https://doi.org/10.1029/2020GL087942

Hoskins, B.J., James, I.N., White, G.H., 1983. The shape, propagation and mean-flow interaction of large-scale weather systems. *Journal of the Atmospheric Sciences* **40**, 1595–1612.

[International Atomoic Energy Agency / World Meteorology Organization (IAEA/WMO)] 2015. Global Network of Isotopes in Precipitation. The GNIP Database. https://www.iaea.org/services/networks/gnip.

Kieser, W.E., Zhao, X.L., Clark, I.D., Cornett, R.J., Litherland, A.E., Klein, M., Mous, D.J.W., Alary, J.F., 2015. The André E. Lalonde AMS Laboratory—the new accelerator mass spectrometry facility at the

University of Ottawa. *Nuclear Instruments and Methods in Physics Research Section B: Beam Interactions with Materials and Atoms* **361**, 110–114.

Koerner, R.M., 1977. Ice thickness measurements and their implications with respect to past and present ice volumes in the Canadian High Arctic ice caps. *Canadian Journal of Earth Sciences* **14**, 2697–2705.

Lacelle, D., 2011. On the $\delta^{18}O$, δD and D-excess relations in meteoric precipitation and during equilibrium freezing: theoretical approach and field examples. *Permafrost and Periglacial Processes* **22**, 13–25.

Lachenbruch, A.H., 1962. Mechanics of thermal contraction cracks and ice-wedge polygons in permafrost. *Geological Society of America Special Paper* **70**, 1–66.

Lachniet, M.S., Lawson, D.E., Sloat, A.R., 2012. Revised 14C dating of ice wedge growth in interior Alaska (USA) to MIS 2 reveals cold paleoclimate and carbon recycling in ancient permafrost terrain. *Quaternary Research* **78**, 217–225.

Lauriol, B., Duchesne, C., Clark, I.D., 1995. Systematique du remplissage en eau des fentes de gel: les resultats d'une etude oxygene-18 et deuterium. *Permafrost and Periglacial Processes* **6**, 47–55.

Lecavalier, B.S., Fisher, D.A., Milne, G.A., Vinther, B.M., Tarasov, L., Huybrechts, P., Lacelle, D., Main, B., Zheng, J., Bourgeois, J., Dyke, A.S., 2017. High Arctic Holocene temperature record from the Agassiz ice cap and Greenland ice sheet evolution. *Proceedings of the National Academy of Scinces USA* **114**, 5952–5957.

Lemmen, D.S., 1989. The last glaciation of Marvin Peninsula, northern Ellesmere Island, High Arctic, Canada. *Canadian Journal of Earth Sciences* **26**. http://dx.doi.org/10.1139/e89-220.

Lewkowicz, A.G., 1994. Ice-wedge rejuvenation, Fosheim Peninsula, Ellesmere Island, Canada. *Permafrost and Periglacial Processes* **5**, 251–268.

Liljedahl, A.K., Boike, J., Daanen, R.P., Fedorov, A.N., Frost, G. V., Grosse, G., Hinzman, L.D., *et al.*., 2016. Pan-Arctic ice-wedge degradation in warming permafrost and its influence on tundra hydrology. *Nature Geoscience* **9**, 312–318.

Mackay, J.R., 1974. Ice-wedge cracks, Garry Island, Northwest Territories. *Canadian Journal of Earth Sciences* **11**, 1366–1383.

Mackay, J.R., 1990. Some observations on the growth and deformation of epigenetic, syngenetic and anti-syngenetic ice wedges. *Permafrost and Periglacial Processes* **1**, 15–29.

Mackay, J.R., 1992. The frequency of ice-wedge cracking (1967–1987) at Garry Island, western Arctic coast, Canada. *Canadian Journal of Earth Sciences* **29**, 236–248.

Mackay, J.R., 1993. Air temperature, snow cover, creep of frozen ground, and the time of ice-wedge cracking, western Arctic coast. *Canadian Journal of Earth Sciences* **30**, 1720–1729.

Mackay, J.R., 2000. Thermally induced movements in ice-wedge polygons, western Arctic coast: a long-term study. *Géographie physique et quaternaire* **54**, 41.

Murseli, S., Middlestead, P., St-Jean, G., Zhao, X., Jean, C., Crann, C.A., Kieser, W.E., Clark, I.D., 2019. The Preparation of Water (DIC, DOC) and Gas (CO 2, CH 4) Samples for radiocarbon analysis at AEL-AMS, Ottawa, Canada. *Radiocarbon* **61**, 1563–1571.

Peros, M.C., Gajewski, K., 2008. Holocene climate and vegetation change on Victoria Island, western Canadian Arctic. *Quaternary Science Reviews* **27**, 235–249.

Pollard, W.H., 1991. Observations on massive ground ice on Fosheim Peninsula, Ellesmere Island, Northwest Territories. Ottawa. Current Research, Part E. Geological Survey of Canada Paper no. 91-1E, p. 223–231, https://doi.org/10.4095/132647

Pollard, W.H., 2000. Distribution and characterization of ground ice on Fosheim Peninsula, Ellesmere Island, Nunavut. In: Garneau, M., Alt, B.T. (Eds.), *Environmental Response to Climate Change in the Canadian High Arctic. Geological Survey of Canada Bulletin* 529, 207–233.

Pollard, W., Ward, M., Becker, M., 2015. The Eureka Sound lowlands: an ice-rich permafrost landscape in transition. In: 68^{e} Conférence Canadienne de Géotechnique et 7^{e} Conférence Canadienne sur le Pergélisol, September 20–23, 2015, Québec.

Reimer, P.J., Bard, E., Bayliss, A., Beck, J.W., Blackwell, P.G., Ramsey, C.B., Buck, C.E., *et al.*, 2013. IntCal13 and Marine13 radiocarbon age calibration curves 0–50,000 years cal BP. *Radiocarbon* **55**, 1869–1887.

Riseborough, D., Smith, M., 1998. Exploring the limits of permafrost. In: Lewkowicz, A.G., Allard, M. (Eds.), Permafrost: Seventh International Conference. Yellowknife, Canada. Collection Nordicana No. 57 Pages 935–941.

St-Jean, G., 2003. Automated quantitative and isotopic (^{13}C) analysis of dissolved inorganic carbon and dissolved organic carbon in continuous-flow using a total organic carbon analyser. *Rapid Communications in Mass Spectrometry* **17**, 419–428.

St-Jean, M., Lauriol, B., Clark, I.D., Lacelle, D., Zdanowicz, C., 2011. Investigation of ice-wedge infilling processes using stable oxygen and hydrogen isotopes, crystallography and occluded gases (O_2, N_2, Ar). *Permafrost and Periglacial Processes* **22**, 49–64.

Stuiver, M., Polach, H.A., 1977. Reporting of ^{14}C data. *Radiocarbon* **19**, 355–363.

Tanski, G., Couture, N., Lantuit, H., Eulenburg, A., Fritz, M., 2016. Eroding permafrost coasts release low amounts of dissolved organic carbon (DOC) from ground ice into the nearshore zone of the Arctic Ocean. *Global Biogeochemical Cycles* **30**, 1054–1068.

Ward Jones, M.K., Pollard, W.H., Amyot, F., 2020. Impacts of degrading ice-wedges on ground temperatures in a high Arctic polar desert system. *JGR Earth Surface* **125**. http://dx.doi.org/10.1029/2019JF005173.

Washburn, A.L., 1980. Permafrost features as evidence of climatic change. *Earth-Science Reviews* **15**, 327–402.

Williams PJ, Smith MW. 1989. *The Frozen Earth: Fundamentals of Geocryology*. Cambridge, UK: Cambridge University Press.

https://doi.org/10.1017/qua.2020.126 Published online by Cambridge University Press